2132 *Chem. Mater.* **2010,** *22,* 2132–2137
DOI:10.1021/cm902625v

CHEMISTRY OF MATERIALS
Article

Writing Self-Assembled Mesostructured Films with In situ Formation of Gold Nanoparticles

Luca Malfatti,[†] Daniela Marongiu,[†] Stefano Costacurta,[‡] Paolo Falcaro,[§] Heinz Amenitsch,[⊥] Benedetta Marmiroli,[⊥] Gianluca Grenci,[#] Maria Francesca Casula,[||] and Plinio Innocenzi*[,†]

[†]*Laboratorio di Scienza dei Materiali e Nanotecnologie (LMNT), CR-INSTM, Università di Sassari Palazzo Pou Salid Piazza Duomo 6, 07041 Alghero SS, Italy,* [‡]*Associazione CIVEN, Via delle Industrie 5, 30175 Venezia, Italy,* [§]*CSIRO, Division of Materials Science and Engineering, Private Bag 33, Clayton South MDC, Victoria 3169, Australia,* [⊥]*Institute of Biophysics and Nanosystems Structure Research, Austrian Academy of Sciences, Schmiedlstrasse 6, 8042, Graz, Austria,* [#]*TASC, INFM National Laboratory, S.S. 14, Km163.5 in Area Science Park, 34012 Basovizza, Trieste, Italy, and* [||]*Dipartimento di Scienze Chimiche and INSTM, Università di Cagliari, 09042 Cagliari, Italy*

Received August 25, 2009. Revised Manuscript Received January 29, 2010

We have developed an integrated technology that allows patterning and formation of gold-nanoparticles in self-assembled mesoporous films in a single step; this technique allows fabrication of patterned structures with high aspect ratios in a direct, simple, and reproducible way. We have used high intensity X-rays that interact with the mesoporous matrix through different processes, by removing the organic templates, increasing the polycondensation of the organic−inorganic silica network, and partially removing the methyl groups bonded in the hybrid matrix. The final material, after patterning and chemical etching, exhibits gold nanoparticles of few nanometers homogeneously dispersed in the porous matrix.

Introduction

Bottom-up nanofabrication of materials that self-assemble into well-defined morphologies, shapes, and patterns is a leading trend in nanotechnologies; it remains, however, a gap to be filled for practical exploitation in devices, which is the integration with top-down technologies. Functional nanostructures need to be fabricated with a specific design and must be compatible with the current lithographic technologies. Full development of self-assembled nanomaterials into new applications could be envisaged in a short time only if this gap will be soon fulfilled. An impressive number of patterning technologies, both top-down and bottom-up, have been developed in these last years as soon as new nanostructured materials have been synthesized.[1] An almost customized palette of technologies is nowadays available for patterning nanomaterials but generally several complicate fabrication steps are required and seldom are able to integrate different technological solutions.[2] Top-down lithographic techniques are generally based on application of a writing beam, such as UV light, X-rays, electrons, to a material that responds to the radiation. The writing process can be direct or used for preparing a mold and to pattern through replica. Bottom-up preparation of nanostructured films is more compatible with soft-lithography techniques, such as MIMIC[3,4] or dip-pen nanolithography,[5,6] but these techniques appear at the moment not well integrated with the current technologies of mass production, which are mainly top-down. It is, however, important not to lose the opportunity represented by nanochemistry that allows preparing self-assembled materials with new properties and functions, which is impossible to obtain by top-down materials processing.[7] X-rays are among the most common writing tools for patterning thin films of different types. In previous works, we have demonstrated that by using high-energy X-rays, it is possible to achieve a direct writing of different types of materials, such as self-assembled mesoporous films[8,9] and sol−gel processed materials.[10] The technique is surprisingly effective for writing in a direct and very simple way films of different materials and is highly reproducible. Deep X-ray

*Corresponding author. E-mail: plinio@uniss.it.

(1) Innocenzi, P.; Kidchob, T.; Falcaro, P.; Takahashi, M. *Chem. Mater.* **2008**, *20*, 607.
(2) Gates, B. D.; Xu, Q.; Stewart, M.; Ryan, D.; Willson, C. G.; Whitesides, G. M. *Chem. Rev.* **2005**, *105*, 1171.
(3) Kim, E.; Xia, Y.; Whitesides, G. M. *Nature* **1995**, *376*, 581.
(4) Kim, E.; Xia, Y.; Whitesides, G. M. *J. Am. Chem. Soc.* **1996**, *118*, 5722.
(5) Piner, R.; Zhu, J.; Xu, F.; Hong, S.; Mirkin, C. A. *Science* **1999**, *283*, 661.
(6) Salaita, K.; Wang, Y.; Mirkin, C. A. *Nat. Nanotechnol.* **2007**, *2*, 145.
(7) Ozin, G. A.; Cademartiri, L. *Small* **2009**, *11*, 1240.
(8) Falcaro, P.; Costacurta, S.; Malfatti, L.; Takahashi, M.; Kidchob, T; Casula, M. F.; Piccinini, M.; Marcelli, A.; Marmiroli, B.; Amenitsch, H.; Schiavuta, P.; Innocenzi, P. *Adv. Mater.* **2008**, *20*, 1864.
(9) Malfatti, L; Kidchob, T.; Costacurta, S.; Falcaro, P.; Schiavuta, P.; Amenitsch, H.; Innocenzi, P. *Chem. Mater.* **2006**, *18*, 4553.
(10) Falcaro, P.; Malfatti, L.; Vaccari, L.; Amenitsch, H.; Marmiroli, B.; Grenci, G.; Innocenzi, P. *Adv. Mater.* **2009**, *21*, 4932.

 Published on Web 03/01/2010

lithography (DXRL) is generally used to produce microstructures with high aspect ratio;[11−14] even if DXRL requires highly brilliant sources such as synchrotron light, the technique shows some distinctive advantages with respect to other lithographic technologies, such as the possibility of fabricating high aspect ratio structures of very good quality and small surface roughness.[15] High-aspect-ratio materials can be easily obtained in a microscale but the potentiality of application of the technique extends to the nanoscale.[16,17] DXRL has been already employed to produce gold-ruby glasses using two fabrication steps: irradiation of glass samples containing a gold precursor and annealing at 500 °C.[1] We have thought, therefore, that this technique could be extended to produce functional nanomaterials containing nanoparticles, we have therefore applied deep X-ray lithography to fabricate complex patterned microstructures formed by gold nanoparticles embedded in a mesoporous matrix. Even if several techniques for writing mesoporous,[18] hybrid polymeric, and oxide films have been reported so far, the technique that we have developed appears direct, simple and shows a high integration of bottom-up and top-down technologies.

The fabrication of gold-doped arrays of high surface area can find a direct application as optical transducers for analytical techniques focused on biological detection such as surface plasmon resonance,[19,20] ultrafast nonlinear optical response,[21] surface plasmon field-enhanced fluorescence spectroscopy,[22] and surface enhanced Raman scattering spectroscopy.[23] The presence of gold nanoparticles at the interface between a biological analyte and the porous matrix, in fact, should allow a strong increase in the detection signal due to a collective oscillation of conduction electrons of the metal nanoparticles (plasmon). In principle the DXRL allows fabricating an array of mesoporous pillars with a diameter of 200−300 nm that contain metallic nanoparticles into the pores.

Experimental Section

Pluronic F127 ($OH(CH_2-CH_2O)_{106}(CHCH_3CH_2O)_{70}(CH_2-CH_2O)_{106}H$), tetraethylorthosilicate (TEOS), methyltriethoxysilane (MTES), and ethanol (EtOH) were purchased from Aldrich and used as received. Tetrachloroauric(III) acid hydrate, $HAuCl_4$, was used as gold precursor (ABCR). Silica glass slides and (100) oriented, P-type/Boron doped silicon wafers were employed as the substrates. A precursor sol containing the silica source (mother solution) was prepared by adding in the following order: EtOH, TEOS, MTES, and aqueous HCl in the molar ratios $Si:EtOH:H_2O:HCl = 1:2.78:1.04:1.4 \times 10^{-2}$, where "Si" stands for a mixture of TEOS and MTES whose molar ratio c = [MTES]/[TEOS] was set to 0.5. This sol was stirred for one hour at room temperature, to prehydrolyze the silicon alkoxides. Another solution (templating solution) was prepared dissolving 1.3 g of Pluronic F127 in a mixture of 15 cm^3 EtOH and 1.5 cm^3 acid aqueous solution (5.7×10^{-2} M). The final precursor sol, which was obtained by adding 7.7 cm^3 of the mother solution to the templating solution, was reacted under stirring for further 24 h. Tetrachloroauric(III) acid hydrate was dissolved in the TEOS-MTES-surfactant sol and a transparent yellow solution was finally obtained. The final molar ratios were $Si:EtOH:H_2O:HCl:F127:HAuCl_4 = 1:16.3:5.4:1.9 \times 10^{-2}:5 \times 10^{-3}:3.7 \times 10^{-3}$. The silicon substrates were dip-coated in the precursor sol at 5 mm s^{-1} pulling rate and 30% relative humidity (RH), the films were exposed to X-rays immediately after the deposition.

The films were patterned using the Deep X-ray Lithography beamline (DXRL) at Elettra synchrotron facility (Trieste, Italy). The samples were exposed through X-ray masks containing test patterns of different size, shape, and geometry (5−500 μm). The masks had a gold absorber 20 μm thick and a titanium transparent membrane with thickness of 2.2 μm. X-ray doses in the 0.8−14 kJ cm^{-3} range were used for patterning. The etching solution was prepared by a mixture of ethanol (15 cm^3), ethylene glycol (30 cm^3), and water (1 cm^3). The solution was optimized to obtain the etching in a time scale of 5 min and the maximum aspect ratio for the patterned structures. The developed films were rinsed with EtOH and dried under a nitrogen flow. For TEM measurements some samples were thermally treated after etching for 10 min at 250 °C.

The organization of the porous structure was investigated by 2D grazing incidence small-angle X-ray scattering (GISAXS) at the Austrian SAXS beamline at Elettra. The incident energy was set at 8 keV (λ = 1.54 Å). The instrumental glancing angle between the incident radiation and the sample was set slightly above the critical angle, which is typical of grazing incidence mode. A 2D CCD detector (Photonic Science, U.K.) was used to acquire the scattering patterns.

Transmission electron microscopy (TEM) images were obtained in bright-field mode on a JEOL 200CX microscope equipped with a tungsten cathode operating at 200 kV. Samples were prepared by evaporation on a carbon-coated copper grid of one drop of a suspension containing scratched fragments of the films in n-octane. Characteristic center-to-center pore distance of the film was obtained by line profile analysis performed on representative TEM pictures using ImageJ program. This value was calculated as the average full width at half-maximum (FWHM) of the intensity distribution along a line passing through the pore centers. Line profile analysis was done on different regions of the TEM micrograph and the obtained values were averaged to give a more accurate result. Nanoparticle size estimation and distribution were automatically obtained by using a specific routine running on IgorPro; a squared region of 1024 × 1024 or 512 × 512 pixels was taken from TEM pictures and used for the analysis. A Wallis filter was applied to these regions to produce a better local contrast throughout the image by reducing the overall contrast between bright and dark areas.

Infrared spectra were collected using a Bruker Hyperion 3000 microscope attached to a Bruker Vertex 70 interferometer working in the mid-IR range with a conventional Globar source and a

(11) Ehrfeld, W.; Lehr, H. *Radiat. Phys. Chem.* **1995**, *45*, 349.
(12) Ehrfeld, W.; Schmidt, A. *J. Vac. Sci. Technol., B* **1998**, *16*, 3526.
(13) Hruby, J. *MRS Bull.* **2001**, 337.
(14) Kupka, R. K.; Bouamrane, F.; Cremers, C.; Megtert, S. *Appl. Surf. Sci.* **2000**, *164*, 97.
(15) Noda, D.; Tanaka, M.; Shimada, K.; Yashiro, W.; Momose, A.; Hattori, T. *Microsyst. Technol.* **2008**, *14*, 1311.
(16) Ehrfeld, W.; Hessel, V.; Löwe, H.; Schulz, C.; Weber, L. *Microsyst. Technol.* **1999**, *5*, 105.
(17) Meyer, P.; Schulz, J.; Hahn, L.; Saile, V. *Microsyst. Technol.* **2008**, *14*, 1491.
(18) Innocenzi, P.; Kidchob, T.; Falcaro, P.; Takahashi, M. *Chem. Mater.* **2008**, *20*, 607.
(19) Anker, J. N.; Hall, W. P.; Lyandres, O.; Shah, N. C.; Zhao, J.; Van Duyne, R. P *Nat. Mater.* **2008**, *7*, 442.
(20) Smith, E. A.; Corn, R. M. *Appl. Spectrosc.* **2003**, *57*, 320A.
(21) Gu, J; Shi, J.; You, G.; Xiong, L.; Qian, S.; Hua, Z.; Chen, H. *Adv. Mater.* **2005**, *17*, 557.
(22) Liebermann, T.; Knoll, W. *Colloids Surf., A* **2000**, *171*, 115.
(23) Nie, S.; Emory, S. R. *Science* **1997**, *275*, 1102.

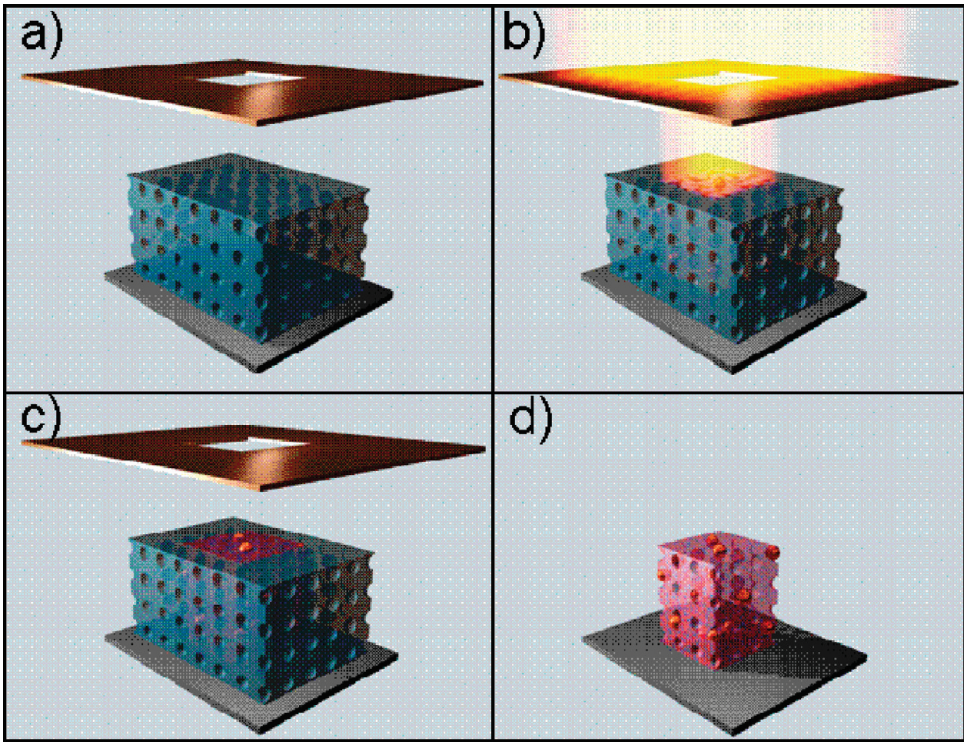

Figure 1. Illustration of the integrated top-down and bottom-up lithographic process. (a) The mesostructured film that contains the gold precursor and the templating micelles is (b) exposed just immediately after the deposition to a X-ray beam through a mask. (c) X-rays remove the template, condense the inorganic pore walls, and promote the formation of gold-nanoparticles within the porous organized matrix of the film. (d) Chemical etching allows removing of the unexposed part of the film.

KBr beamsplitter. The microscope was equipped with a liquid-nitrogen-cooled MCT (mercury−cadmium−telluride) detector and a motorized sample stage that allowed mapping of the samples using a rectangular aperture of $10 \times 10\,\mu$m. Each spectrum was obtained in transmission mode averaging 512 interferograms at a resolution of 16 cm^{-1}. Samples were observed by an optical microscope Nikon Optiphot 500 both before and after the development.

SEM imaging was performed with a Zeiss Supra 40 instrument (Carl Zeiss MicroImaging GmbH, Germany) using secondary electrons as measuring signal.

The SEM was equipped with an EDS (Energy dispersive X-ray spectroscopy) system (EDAX Inc., NY) with a nominal resolution of 140 eV. EDS is a technique that permits to obtain a qualitative and quantitative detection of the chemical elements. With this system a mapping of gold and silicon was performed in the samples after etching.

An atomic force microscope (NT-MDT Ntegra) was used to analyze the topography of the samples. Surfaces were measured at 0.5−1 Hz scan speed in semicontact mode, using a silicon tip with nominal resonance frequency of 150 kHz, 5 N m^{-1} force constant, and 10 nm typical curvature radius.

X-ray diffraction (XRD) measurements were recorded by a Bruker D8 diffractometer equipped with a scintillator counter. The Cu KR radiation was used to perform an $\omega/2\theta$ scan from 30 to 85° with a resolution of 0.02°. The optical absorption spectra were collected on films deposited on fused silica substrates using a Nicolet Evolution 300 spectrophotometer in the wavelength range 200−900 nm with a scan speed of 500 nm min^{-1}. Each spectrum is the average of three scans collected with a bandwidth of 1.5 nm.

Results and Discussion

We have used an integrated top-down and bottom-up technology to obtain complex lithographic patterns of mesoporous materials doped with gold nanoparticles; the overall process is illustrated in Figure 1. The mesostructured film, which contains the gold precursor and the templating micelles (Figure 1a), is exposed to X-rays through a mask just immediately after the deposition (Figure 1b). The effect of X-rays is to remove the template, to condense the inorganic pore walls and finally to promote the formation of gold nanoparticles within the porous matrix of the films (Figure 1c); the final processing step is the chemical etching that allows removing the unexposed part of the film (Figure 1d). The highly energetic X-rays are used as an efficient writing tool that plays a multiple effect on the mesostructured films. Furthermore, as we have already demonstrated in previous works, the exposure to an intense X-ray source does not disrupt the mesophase, even after the removal of the surfactant template.[8] By adjusting the dose it is possible to change the X-rays effect on the materials, therefore controlling some of the properties. Figure 2 shows the bright-field images of as-deposited mesostructured films exposed to different X-ray doses: 2.8 kJ cm^{-3} (Figure 2a) and 14 kJ cm^{-3} (Figure 2b); gold nanoparticles, which appear as dispersed black dots in the TEM images, are directly formed after exposure to X-rays. A higher dose promotes the formation of a larger amount of gold nanoparticles, which have similar dimensions (within the experimental error) as indicated by TEM images: 5.6 ± 1.8 nm at 14 kJ cm^{-3} and 6.5 ± 1.8 nm at 2.8 kJ cm^{-3}. The same samples have been treated at 250 °C to observe also the mesopores (Figure 2c, d); as-deposited films have, in fact, a low electronic contrast that does not allow a direct observation

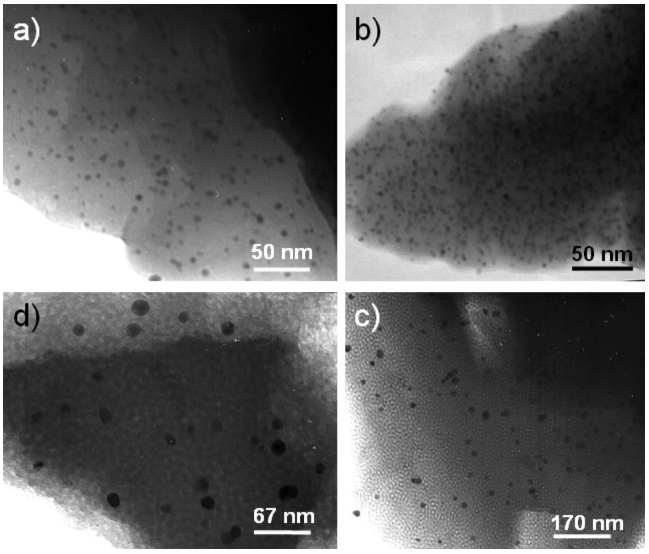

Figure 2. Bright-field TEM images of as deposited mesostructured films exposed to different X-ray doses: (a) 2.8 and (b) 14 kJ cm^{-3} doses. (c, d) Same samples after thermal treatment to 250 °C.

of the organized mesostructure; the pore dimension estimated from the TEM images has been calculated to be 6.7 ± 1.8 nm, which is in the same order of magnitude of gold nanoparticles before thermal treatment. After thermal treatment the gold nanoparticles grow and assume a broader size distribution. We have obtained an averaged particle size of 14.6 ± 4.0 and 13.7 ± 5.1 nm from TEM images c and d in Figure 2, respectively. The particle size distribution of the four TEM pictures shown in Figure 2 are reported in Figure S1 of the Supporting Information.

The deep X-rays lithographic process produces well-defined patterns even in the case of complex shapes; the optical images in Figure 3a,b and c show some examples of these different patterns. The optical images are taken from as deposited films on silicon after exposure to X-rays and before etching. The pink-red color is indicative of the presence of gold nanoparticles, while the unexposed part of the film appears light blue. The same pattern of Figure 3c after etching is shown in the SEM image in Figure 3d; the pattern appears highly regular with a good aspect-ratio.

The quality of the process, which allows obtaining defined patterns and mesoporous arrays doped with gold nanoparticles, is clearly demonstrated by EDS images of a patterned film. Figure 4 shows the SEM image of a patterned microstructure on silicon substrate after etching (Figure 4a) and the EDS images obtained by measuring the signals of gold (Figure 4b) and silicon (Figure 4c). A darker color is correlated with a lower signal intensity; the Au signal is observed in the developed part of the film, whereas the Si signal, which is given by the silicon substrate, is more intense in the etched. The EDS signal of gold appears homogeneous and indicates that gold nanoparticles are well dispersed and distributed in the sample.

The optical images of a gold-doped patterned mesostructure deposited on glass slide after etching (Figure 5a, b) show that the final material is highly defined and homogeneous. The quality of the process, which includes

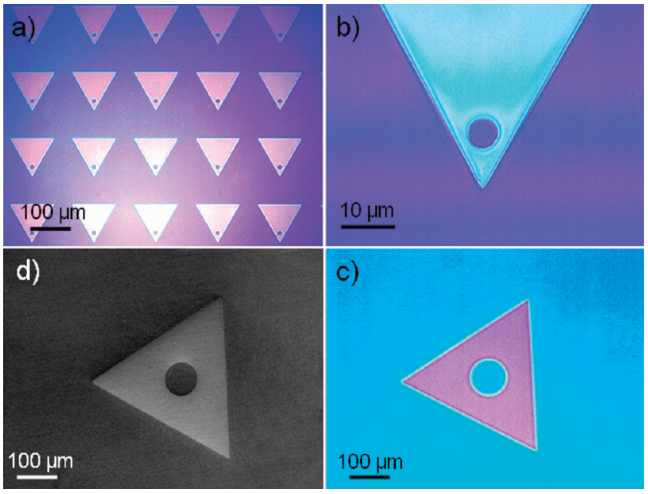

Figure 3. Optical images taken from as deposited films on silicon after exposition to X-rays and before etching. The pink-red color is indicative of the presence of gold nanoparticles, whereas the unexposed part of the film appears light blue. The same pattern of image c after etching is shown in the SEM image in d.

the chemical etching, has been evaluated by AFM analysis. Figure 5c,d shows the AFM images on 80×80 μm and 50×50 μm areas of a patterned sample on silicon substrate. The developed microstructures show a height of ~600 nm with a sharp profile; the possibility to pattern films thicker than 0.5 μm is a clear advantage of deep X-ray lithography. It is, in fact, possible to fabricate complex patterns with a sharp profile and a high aspect ratio; the high energy of the X-rays allows achieving a homogeneous and deep lithography even in very thick films, which is not possible to obtain with other common techniques such as soft X-rays or UV light.

The high energy X-rays on the material have different effects, we have seen that they promote a fast and direct formation of gold nanoparticles in the exposed part of the films, but they also affect its structure. The effect is simultaneous and clearly the kinetics of the different processes involved must be well balanced to obtain functional materials with tunable properties on a nanoscale. In the present case we have obtained a mesopores array (see GISAXS pattern in Figure S2 of the Supporting Information) containing gold particles of few nanometers. The material mesostructure is not affected by X-rays exposure and etching; in particular etching, which is generally a very critical step, is easy and fast and is based on the fact that the exposed part of the film is preferentially densified by effect of X-rays. Even if the mechanism is not clear we suppose, in according to the literature, that the formation of radical species induced by X-rays promotes the densification of silica via silanols condensation reactions. This is somehow similar to what observed when sol–gel films are exposed to UV light or soft X-rays, which produce a similar condensation effect, even if it is not so extended such as after exposure to very energetic X-rays.[24] The free radicals, H· and OH·, are formed

(24) Imai, H. In *Handbook of Sol–Gel Science and Technology*; Sakka, S., Kozuka, H., Eds.; Kluwer Academic Publishers: New York, 2004; Vol. *I*, pp 639–550.

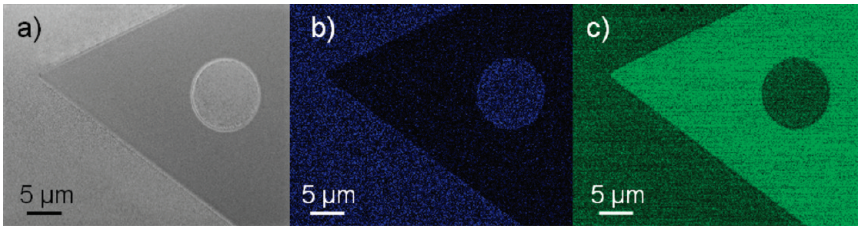

Figure 4. SEM image of (a) a patterned microstructure on silicon substrate after etching and the EDS images obtained by measuring the signals of (b) gold and (c) silicon. A darker color is correlated with a lower signal intensity.

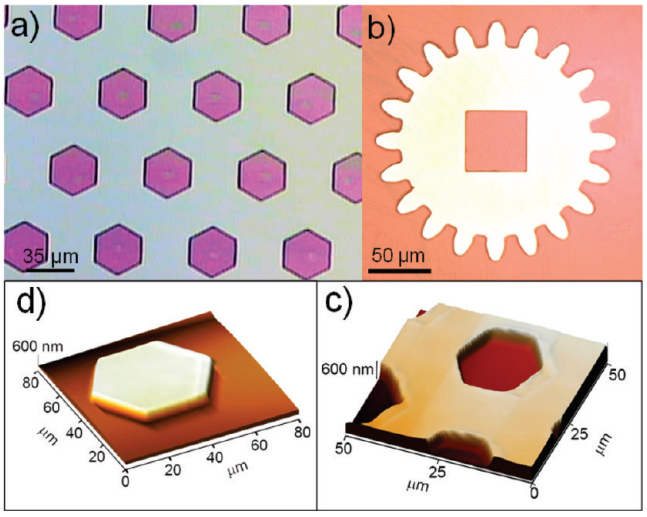

Figure 5. (a, b) Optical images of a gold-doped patterned mesostructures deposited on glass slide after etching. AFM images on (c) 50 × 50 and (d) 80 × 80 μm^2 areas of a patterned sample on silicon substrate.

by dissociation of water molecules exposed to ionization radiation.[25] Residual adsorbed water is always present in sol−gel and mesoporous films and is the source of the free radicals. Besides promoting densification of the inorganic walls and depolymerization of the organic template, the same radicals are also responsible for the gold reduction;[26] the hydrogen radicals act as electron donors to reduce the $HAuCl_4$ to metallic gold through the reactions[26,27]

$$HAuCl_4 \rightarrow H^+ + AuCl_4^- \quad (1)$$

$$H_2O \rightarrow H^\cdot + OH^\cdot \quad (2)$$

$$4OH^\cdot \rightarrow 2H_2O + O_2 \quad (3)$$

$$AuCl_4^- + 3H^\cdot \rightarrow Au + 3H^+ + 4Cl^- \quad (4)$$

A side product of this reaction is HCl, which could have some local densification effect even if its contribution to total condensation of the matrix is negligible. The intensity of the dose, as we have shown, is a critical parameter, because it controls the degree of condensation of the pore

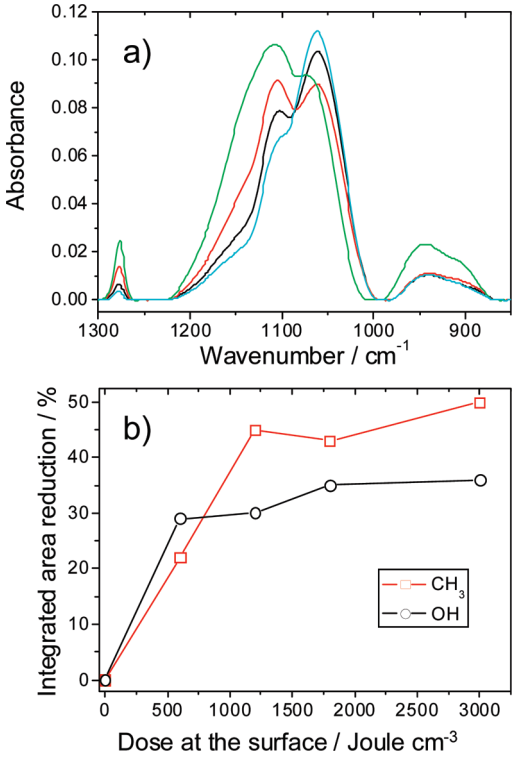

Figure 6. (a) FTIR absorption spectra in the 1300−850 cm^{-1} range of the hybrid films before and after exposure to different X-ray doses: green line, as deposited; red line, 0.6 kJ cm^{-3}; black line, 1.8 kJ cm^{-3}; cyan line, 3 kJ·cm^{-3}; (b) integrated area reduction (%) of the CH_3 and Si−OH bands as a function of the exposure dose.

walls and the formation of gold nanoparticles. It should be underlined that the exposure of the matrix to X-rays produces different and simultaneous effects: (1) removal of the surfactant (see ref 8 and the Supporting Information), (2) densification of the silica pore walls, (3) partial removal of the methyl groups that are covalently bonded to silicon in the hybrid matrix, and (4) formation of gold nanoparticles. Figure 6a shows the FTIR absorption spectra in the 1300−850 cm^{-1} range of the hybrid films before and after exposure to increasing X-ray doses. The spectra show some distinct absorption bands, one of small intensity which is peaking around 1275 cm^{-1} and is attributed to Si-CH_3 symmetric deformation;[28] a second wide and intense band around 1050 cm^{-1} which is assigned to Si−O−Si antisymmetric stretching,[29] this band is overlapped to another intense band peaking

(25) Belloni, J.; Mostafavi, M.; Remita, H.; Marignier, J H.; Delcourt, M. O. *New J. Chem.* **1998**, 1239–1255.
(26) Wang, C. H.; Hua, T. E.; Chien, C. C.; Yu, Y. L.; Yang, T. Y.; Liu, C. J.; Leng, W. H.; Hwua, Y.; Yang, Y. C.; Kim, C. C.; Je, J. H.; Chen, C. H.; Lin, H. M.; Margaritondo, G. *Mater. Chem. Phys.* **2007**, *106*, 323–329.
(27) Gachard, E.; Remita, H.; Khatouri, J.; Keita, B.; Nadjo, L.; Belloni, J. *New J. Chem.* **1998**, 1257–1265.
(28) Colthup, N. B.; Daly, L. H.; Wiberley, S. E. *Introduction to Infrared and Spectroscopy*; Academic Press: San Diego, 1998.
(29) Innocenzi, P. *J. Non-Cryst. Solids* **2003**, *316*, 309.

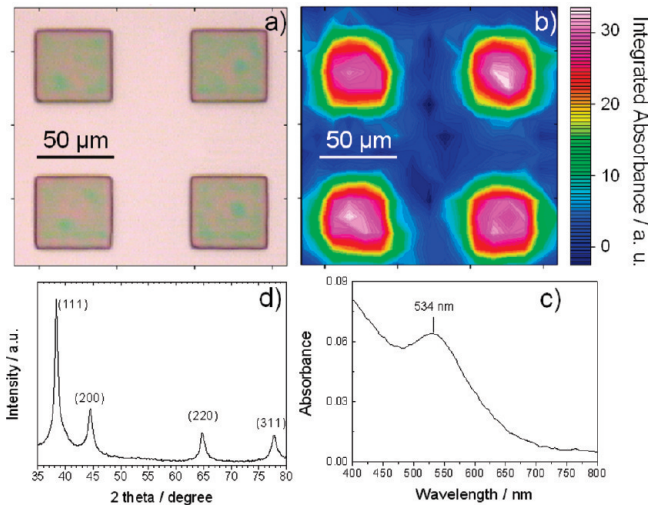

Figure 7. (a) Optical image of a patterned and etched film deposited on silicon substrate; (b) corresponding infrared image obtained by integrating the absorbance relative to the Si−O−Si band. (c) Typical UV−vis absorption spectrum and (d) X-ray diffraction pattern of a mesostructured film deposited on cover-glass slide and exposed to a 14 kJ cm^{-3} X-ray dose.

around 1100 cm^{-1} that is assigned to unreacted alkoxy species[29] and the third one around 950 cm^{-1}, which is assigned to Si−OH. The CH_3 and Si−OH bands decrease in intensity with the increase of the X-rays exposure dose and give a direct indication of the effect of synchrotron light on the organic components within the films and on silica condensation. We have calculated the change of the integrated area of the CH_3 and Si−OH bands as a function of the exposure dose, taking as reference the band of the as-deposited sample. Figure 6b shows the change of the integrated area of the CH_3 and Si−OH bands: higher doses induce a larger densification and a removal of organic groups, which is clearly shown by the progressive disappearing of the overlapped band because of unreacted alkoxides at 1100 cm^{-1} with the increase in the X-ray dose[29] (Figure 6a).

We have also used infrared imaging as a powerful characterization tool to evaluate the effect of X-rays on the film. Figure 7a shows the optical image of a patterned and etched film deposited on a silicon substrate. The correspondent infrared image obtained by integrating the absorbance of the Si−O−Si vibrational band (1250−980 cm^{-1}) is shown in Figure 7b. The infrared image shows that the patterned areas are formed by silica whose signal is not observed in the etched areas, indicating that the chemical etching process is really effective in removing from the substrate the part of the film that has not been exposed to X-rays. Typical UV−vis absorption spectrum and X-ray diffraction pattern of a mesostructured film deposited on cover-glass slide and exposed to 14 kJ cm^{-3} X-ray dose are shown in panels c and d in Figure 7, respectively. The UV−vis spectrum shows a plasmonic absorption band peaking at 534 nm and the X-ray figure the diffraction pattern of metallic gold. They confirm the formation of gold nanoparticles upon X-ray exposure. We have evaluated the size of gold nanoparticles from the plasmonic peak of UV−vis spectra,[30] we have calculated that the average dimension is 5.6 nm, whereas the nanoparticle size is 9.6 ± 3 nm when the Scherrer equation is applied to the X-ray patterns. Both the values are in good agreement with the nanoparticles size measured by electron microscopy.

Conclusions

An integrated combination of top-down and bottom-up technologies has been developed to fabricate complex patterned structures of composite nanomaterials. X-rays induce condensation of the pore walls, remove the surfactant and partially remove the covalently bonded organic groups, at the same time gold nanoparticles are formed in a simple and controlled way; the X-ray dose controls the process. The exposed part of the film is selectively condensed by X-rays to allow a very effective chemical etching and the fabrication of high-aspect-ratio patterns, with sharp walls. This process is versatile and can be applied to different oxides, such as pure silica, titania, zirconia, etc., and different types of hybrid organic−inorganic materials. The process is direct, highly reproducible, and does not need several complicate steps for the fabrication of complex porous patterns which contain nanoparticles of controlled dimensions.

Acknowledgment. Fernando Cacho Nerin is gratefully acknowledged for experimental support. This work was supported by the E.U. through SAXIER Contract 011934.

Supporting Information Available: Particle size distribution of mesostructured films with embedded gold-nanoparticles estimated from TEM measurements. Grazing incidence small-angle X-ray scattering of a mesostructured film with embedded gold nanoparticles after exposure with DXRL (PDF). This material is available free of charge via the Internet at http://pubs.acs.org.

(30) Haiss, W.; Thanh, N. T. K.; Aveyard, J.; Fernig, D. G. *Anal. Chem.* **2007**, *79*, 4215.